Primary cilium cAMP regulates cyclic saltatory neuronal migration at the centrosome

Julie Stoufflet*[1,2], Maxime Chaulet*[1], Mohamed Doulazmi[2], Coralie Fouquet[1], Caroline Dubacq[1], Christine Métin[3], Alain Trembleau[1], Pierre Vincent[2] and Isabelle Caillé[1,4]

1.CNRS UMR8246, Inserm U1130, Sorbonne Université UMCR18, Institut de Biologie Paris Seine (IBPS), Paris, France

2. CNRS UMR8256, Sorbonne Université, Institut de Biologie Paris Seine (IBPS), Paris, France.

3. Inserm UMR-S 839. Institut du Fer à Moulin, Sorbonne Université, Paris, France.

4. Université de Paris, Paris, France

Corresponding author: isabelle.caille@upmc.fr

Summary :

The primary cilium (PC) is crucial for neuronal migration but the underlying cellular mechanisms are mostly unknown. Here, we show that ciliary-produced cAMP present at the centrosome locally activates cAMP-dependent Protein Kinase A (PKA). We analyzed cAMP dynamics through biosensor live-imaging in cyclic saltatory migrating neurons of the mouse postnatal rostral migratory stream. This revealed a dynamic cAMP hotspot cyclically present at the centrosome, thus located at the basis of the PC. Genetic ablation of the PC and knock-down of the ciliary Adenylate Cyclase 3 lead to the hotspot disappearance. They also affect migration with defective centrosome/nucleus coupling leading to altered nucleokinesis, which is recapitulated by PKA genetic delocalization. We thus show that PC and centrosome act as a single signaling unit, linked by ciliary cAMP diffusion regulating the rhythmicity of saltatory migration at the centrosome. We generalized this finding to embryonic and adult migrating neurons.

Keywords: neuronal migration, primary cilium, centrosome, cyclic AMP, live-imaging, FRET-biosensor

INTRODUCTION

Neuronal migration is a crucial step for the establishment of brain circuitry, as all neurons have to migrate from their site of birth to their final site of integration. Dysfunction in neuronal migration leads to severe cortical malformations such as lissencephalies and periventricular or subcortical band heterotopia and might be involved in psychiatric disorders (Bertipaglia et al., 2018; Silva et al., 2019). Most migrating neurons display a cyclic saltatory migration with alternations of somal translocation and pauses. For each somal translocation, nucleus and centrosome move forward in a "two-stroke" cycle, with the centrosome moving first within a swelling in the leading process (centrokinesis, CK) and the nucleus following subsequently (nucleokinesis, NK) (Bellion et al., 2005; Belvindrah et al., 2017; Schaar and McConnell, 2005). Regulation of centrosome dynamics is thus pivotal in the regulation of migration, through microtubular nucleus to centrosome coupling allowing NK (Belvindrah et al., 2017; Jheng et al., 2018; Tanaka et al., 2004; Tsai et al., 2007)

The centrosome is located at the basis of the primary cilium (PC), a small rod-shaped organelle important for migration. It is present on most eukaryotic cells including neurons (Mandl and Megele, 1989). Its absence or dysfunction in ciliopathies lead to severe brain defects, suggesting its major importance for brain development (Hildebrandt et al., 2011; Valente et al., 2014). In some instances, brains from ciliopathy patients present signs of lisencephaly-like phenotypes (Patel and Barkovich, 2002) or subcortical band heterotopia (Juric-Sekhar et al., 2012), suggesting migration defects. Accordingly, several genes known to be mutated in ciliopathies are important regulators of neuronal migration (Guo et al., 2015). Moreover, genetically modified mice with absent or dysfunctional PC display defective migration of neural crest cells (Tobin et al., 2008) and tangentially migrating interneurons (Baudoin et al., 2012; Higginbotham et al., 2012). Altogether, this suggests that the PC is crucial for neuronal migration, but the underlying cellular mechanisms remain mostly unknown.

The cyclic AMP/PKA (cAMP dependent protein kinase A) signaling pathway is a pleiotropic cellular regulator, involved in multiple processes including cell motility (Howe, 2011). It regulates in particular neuronal migration (Haase, 2003; Toriyama et al., 2012). Compartimentalization and specificity of the pathway is ensured by subcellular localization of PKA through diverse AKAPs (A Kinase Anchoring Proteins) (Torres-Quesada et al., 2017).

In migrating cells, PKA was described at the actin-rich leading edge of fibroblasts (Howe et al., 2005) or at the centrosome of lymphocytes T (Ong et al., 2018). In addition, the use of genetically-encoded cAMP specific FRET (Förster Resonance Energy Transfer)-based biosensors in living cells revealed that cAMP itself can be highly compartmentalized at the subcellular level (Calebiro and Maiellaro, 2014; Castro et al., 2014; Lefkimmiatis and Zaccolo, 2014). In neurons, it was described in microdomains of axons, dendrites or growth cones (Averaimo et al., 2016; Calebiro and Maiellaro, 2014; Castro et al., 2010; Maiellaro et al., 2016). In addition, the use of ciliary-targeted FRET-biosensor in fibroblasts and kidney epithelial cells showed that the PC is a cAMP rich microdomain (Moore et al., 2016; Sherpa et al., 2019).

We thus wondered whether the PC could regulate neuronal migration through cAMP dynamics.

Our model for studying neuronal migration is the ventricular/subventricular zone (V/SVZ) to olfactory bulb (OB) migration in the postnatal mouse. In this system, a large quantity of neurons produced in the V/SVZ migrate tangentially by cyclic saltatory migration over a long distance in the Rostral Migratory Stream (RMS) (Lois and Alvarez-BuyIIa, 1994; Lois et al., 1996) (Fig 1A), which allows easy manipulation through intraventricular electroporation followed by live-imaging.

In this model, two-photon imaging of migrating neurons electroporated with a FRET-based biosensor (Epac-S^{H187} (Klarenbeek et al., 2015)) in acute slices of the RMS revealed a dynamic cAMP hotspot localized around the centrosome, present during NK and absent during pauses. Genetic ablation of the PC as well as knock-down of the ciliary Adenylate Cyclase 3 (AC3) induced permanent disappearance of the hotspot, showing the importance of cAMP ciliary production for its formation. The hotspot disappearance led to a slowed-down migration with increased pausing phases and reduced frequency of NK. This was accompanied by defects in centrosome movement with decreased maximum distance from the nucleus and increased uncoupling of centrosome and nucleus. Moreover, genetic delocalization of the centrosomal PKA recapitulated this migratory phenotype, showing its importance as a downstream effector of the cAMP hotspot. Our data thus show that ciliary-produced cAMP forms a dynamic centrosomal hotspot, which locally acts on centrosomal PKA to regulate migration and efficient coupling of centrosome and nucleus. This compartmentalized cAMP dynamics may be widely used in migrating neurons, since we also observed it in radially migrating postnatal OB interneurons, in adult RMS and in radially migrating embryonic cortical neurons.

RESULTS

cAMP dynamics in migrating neurons of the postnatal RMS: a transient centrosomal hotspot during NK

Young neurons migrate in the RMS by alternations of pauses and NK (Fig 1A) (Wichterle et al., 1997).

To investigate cAMP dynamics in migrating neurons, we electroporated neonate mice with an intraventricularly-injected plasmid to express the FRET cAMP-specific biosensor Epac-S^{H187} (fig 1B and 1C). This biosensor displays a high ratio change and excellent photostability for measuring cAMP concentration in the micromolar range (Klarenbeek et al., 2015). Biosensor-expressing neurons were imaged in live acute sections of the RMS with a two-photon microscope (one-hour movies with one-minute intervals). Ratiometric analysis revealed that a cAMP-rich region (hereafter called hotspot) was transiently present during NK and disappeared during pauses (Fig 1D and movie 1 where the same cell is filmed during two successive NK). This hotspot specifically reflected a cAMP local enrichment since it was absent in neurons transfected with a version of Epac-S^{H187} with mutated cAMP binding site (movie 2).

Measurement of the ratiometric characteristics of the hotspot showed that its average diameter was of 965±95nm. In addition, the maximum hotspot ratio level was constant during NK being in average 52% (±2%) higher than the mean cell ratio (n=12 cells performing 16 NK).

Extensive analysis of migrating neurons (ie performing at least one NK during a one-hour movie with NK lasting in average 4.13±0,25min and a pause 12.65±1,25min) showed that 82% of them displayed such a dynamic hotspot (101 neurons performing 134 NK from 10 mice).

The hotspot stereotypically appeared at the front of the cell body before moving into the leading process, where it remained until after the nucleus performed a NK. It then disappeared during the following pause and could reappear later following the same pattern before the neuron undertook another NK.

As this movement resembled the classically described centrosome movement during saltatory migration, we co-electroporated the biosensor with centrin-RFP to label the centrosome (Fig 1E). We saw that the hotspot was present around the centrosome before its movement into the leading process and stayed around it during NK before disappearance during the pause.

Use of a sensitive cAMP biosensor with a high signal to noise ratio coupled with live biphoton imaging in slices thus allowed us to discover a dynamic cAMP hotspot at the centrosome of RMS migrating neurons.

PC is necessary for centrosomal hotspot formation

The PC is a small rod-shaped organelle linked to the centrosome by its axoneme (fig 2A) and involved in neuronal migration (Baudoin et al., 2012; Higginbotham et al., 2012). Intraventricular electroporation of a plasmid expressing GFP allowed labeling of a cohort of migrating neurons in the postnatal RMS. Immunostaining of GFP positive RMS neurons with anti-Arl13B, a ciliary small GTPase, coupled with anti-γ-tubulin, marker of the centrosome, showed that neurons assemble a PC during migration (Fig 2B). The PC length was in average 0,827 ± 0.058µm (N=3 mice, n=50 PC).

Since typical biosensors like ours cannot enter into the PC, some authors specifically targeted biosensors to the PC by fusing them to ciliary proteins and showed that the PC is a cAMP-rich region (Moore et al., 2016; Sherpa et al., 2019). We thus wondered whether the cAMP hotspot that we observed at the centrosome could come from the PC. To answer this question, we used two mouse lines in which deletion of the PC could be genetically induced by Cre recombination. Kif3a is part of a kinesin motor required for cilium maintenance (Rosenbaum and Witman, 2002). Rpgrip1l (retinitis pigmentosa GTPase regulator-interacting protein 1 like) is a protein located at the transition zone of the PC, whose mutation leads to ciliopathies in humans (Arts et al., 2007).

We performed Cre recombination of the floxed genes in migrating RMS neurons by injecting and electroporating a Cre and GFP expressing plasmid into the ventricle of neonate Kif3a$^{lox/lox}$ and Rpgrip1l$^{lox/lox}$ mice (Cre conditions). This was compared to RMS neurons after intraventricular electroporation of a GFP expressing plasmid in the same line of mice (GFP control conditions). Cre electropporation led to an efficient ablation of the PC in both mouse lines: the percentage of GFP positive RMS neurons displaying a γ-tubulin positive centrosome associated with an Arl13B positive PC was significantly reduced in Cre-injected Kif3a$^{lox/lox}$ (25% in Cre versus 68,3% in GFP control animals, n=140 cells from 3 mice in Cre conditions, n=109 cells from 3 mice in control animals, Chi-squared test $p<0.001$) and Rpgrip1l$^{lox/lox}$ mice (16.2% in Cre versus 47% in GFP control animals, n=99 cells from 3 mice for Cre conditions, n=68 cells from 2 mice in controls, Chi-squared test $p<0.001$).

Co-transfection of the cAMP biosensor with Cre in neonate floxed mice showed that cilium ablation led to a concomitant disappearance of the hotspot in both mouse lines (Fig 2C and D and movie 3 and 4). Whereas 82% of cells displayed one hotspot during NK in control mice, this number was reduced to 30% in Cre-transfected Kif3a$^{lox/lox}$ (36 neurons performing 46 NK in 4 mice) and to 20% in Cre-transfected Rpgrip1l$^{lox/lox}$ (52 neurons performing 73 NK in 7 mice) (Fig 2E). When cells displayed two successive NK (as in movie 1), the phenotype of absence or presence of hotspot during NK was persistent. Moreover, the more efficient disappearance of the hotspot in Rpgrip1l recombined neurons as compared to Kif3a recombined neurons is in line with the more efficient genetic ablation of the PC described above, strongly suggesting that the PC is necessary for formation of the hotspot.

Ciliary type 3 Adenylate Cyclase (AC3) is necessary for centrosomal hotspot formation

AC3 is described as the predominant cAMP producer in neuronal PC (Bishop et al., 2007). We thus performed immunohistochemistry in RMS migrating neurons, which revealed AC3 subcellular localization in the PC (Fig 3A). We could not detect any immunoreactivity elsewhere in the cell, suggesting AC3 exclusive localization in the PC. We additionally observed that more than 40% of Arl13B positive primary cilia in the RMS were AC3 positive (n=141 cilia from 2 mice).

We thus used a microRNA targeting AC3 mRNA (coupled to GFP) to knock down (KD) AC3. Its efficiency was verified by qRT-PCR on NIH3T3 cells transfected with miRAC3 or a negative control miR along with a plasmid overexpressing AC3 (Fig 3B). Co-expression of the miRAC3 led to a 40% decrease of the overexpressed AC3 mRNA, as compared to control miR condition, showing efficient KD by miRAC3.

Co-electroporation of the miRAC3 with the biosensor showed that AC3 KD led to similar disappearance of the hotspot as PC ablation (Fig 3C and movie 5). Only 22% (N=2 mice, n=17 cells) of miRAC3 transfected cells displayed a visible hotspot during NK.

This suggests that ciliary AC3 produces the hotspot. Altogether, these results indicate that the PC is the source of the centrosomal hotspot.

Migration defects in the absence of hotspot

Given the dynamics of the hotspot and its subcellular localization at the centrosome, we wondered whether it could regulate migration. We thus compared the migration of control

neurons with the migration of cilium-ablated and AC3 knocked-down neurons, conditions leading to hotspot disappearance. To this end, Kif3a$^{lox/lox}$ neonate mice were intraventricularly transfected with GFP, Cre recombinase coupled with GFP or miRAC3 coupled with GFP. Live acute sections of the RMS were imaged with a confocal microscope (3-hr movies with 3-minute intervals). Tracking of the GFP positive cells showed that cilium ablation as well as AC3 knock-down significantly slowed down migration (GFP 75.49±3.48µm/h versus 55.81±2.74µm/h and 58.08±2.98 µm/h in CRE and miRAC3, $p < 0.001$, GFP: N=3 mice, n=48 neurons, CRE: N=3 mice, n=40 neurons, miRAC3: N=2 mice, n=48 neurons, Fig 4A, movies 6, 7 and 8). This was accompanied by an increased percentage of pausing time (76% in GFP versus 87% and 84% in Cre and miRAC3, $p < 0.001$, GFP: N=3 mice, n=48 neurons, CRE: N=3 mice, n=40 neurons, miRAC3: N=2 mice, n=48 neurons, Fig 4B). Detailed analysis of the NK showed that the average frequency of NK was reduced (3.15±0.21 NK/h in GFP versus 2.06±0.20NK/h and 2.14±0.21NK/h in Cre and miRAC3 $p < 0.001$, GFP: N=3 mice, n=48 neurons, CRE: N=3 mice, n=40 neurons, miRAC3: N=2 mice, n=48 neurons, Fig 4C). The speed and distance of NK were unchanged (not shown). To confirm that the phenotype observed after primary cilium ablation in the kif3a$^{lox/lox}$ mice was due to cilium ablation, we performed the same experiment in the Rpgrip1l$^{lox/lox}$ neonate mice and observed the same defects. The speed was slowed-down (GFP 75.33±2.45 µm/h versus 57.88±2.43µm/h in CRE $p<0.001$, GFP: N=4 mice, n=58 neurons, CRE: N=3 mice, n=80 neurons), the pausing time was increased (77% in GFP versus 85% in CRE, $p<0.001$, GFP: N=4 mice, n=58 neurons, CRE: N=3 mice, n=80 neurons), and the average frequency of NK was reduced (3.23± 0.18 NK/h in GFP versus 2.26± 0.15 NK/h in CRE, $p=0.03$, GFP: N=4 mice, n=58 neurons, CRE: N=3 mice, n=80 neurons) (figure S1).

Altogether, these data suggest that the cAMP produced in PC by ciliary AC3 is necessary for proper neuronal migration.

Defects of centrosome/nucleus coupling in the absence of hotspot

Given the centrosomal location of the hotspot and the above migration defects, we wondered whether the hotspot could directly play a role in centrosome dynamics. To assess this question, we co-transfected centrin-RFP along with GFP, Cre coupled with GFP or miRAC3 coupled with GFP in kif3a$^{lox/lox}$ background and co-tracked cell body and centrosome (movie 9 (GFP) and 10 (CRE)). We defined a centrokinesis (CK) as an increase of the centrosome to nucleus distance of at least 2µm followed by a decrease of at least 2µm.

The maximum distance between nucleus and centrosome during CK was reduced in cilium-ablated and AC3 knocked-down neurons as compared to control GFP neurons (GFP 12.32±0.42µm versus 10.42±0.35µm and 9.85±0.63µm in CRE and miRAC3, $p < 0.001$, GFP: N=3 mice, n=48 neurons, CRE: N=3 mice, n=40 neurons, miRAC3: N=2 mice, n=48 neurons, Fig 5A). Additionally, we defined two types of CK: a CK immediately followed by a NK was considered efficient whereas a CK not followed by a NK was considered inefficient. Interestingly, we saw an increase of the percentage of inefficient CK in cilium ablated and AC3 knocked-down neurons as compared to control GFP neurons (26% in GFP versus 43% and 37% in Cre and miRAC3, $p =0.002$, GFP: N=3 mice, n=48 neurons, CRE: N=3 mice, n=40 neurons, miRAC3: N=2 mice, n=48 neurons, Fig 5B), which suggested that the hotspot was necessary for proper coupling of centrosome and nucleus.

Our results thus suggest that the ciliary dependent hotspot regulates migration by a direct action on the centrosome with consequences on centrosome/nucleus coupling.

Centrosomal PKA is the downstream effector of the hotspot

PKA was described to be localized at the centrosome in certain cell types (Ong et al., 2018; Saade et al., 2017). Immunohistochemical staining for the catalytic subunit of PKA (cPKA) showed that it was indeed the case in RMS migrating cells, where cPKA appeared as a diffuse area surrounding the centrosome (Fig 6A). We then transfected a dominant negative form of PKA (dnPKA) fused with GFP to delocalize PKA from the centrosome (Saade et al., 2017). This dnPKA is a regulatory subunit of PKA, which cannot bind the centrosome and thus traps the endogenous catalytic subunit of PKA in the cytoplasm (Fig 6B). Counting of the percentage of cells displaying visible cPKA immunoreactivity at the centrosome showed that dnPKA efficiently delocalized PKA (26.67% in dnPKA versus 86.05% in GFP, for dnPKA n=30 cells from 2 mice, for GFP n=44 cells from 3 mice).

We thus analyzed the migration and centrosomal dynamics of dnPKA transfected neurons. Similarly to cilium deletion and AC3 knock-down, dnPKA transfection slowed down migration (GFP 75.49±3.48µm/h versus 55.76±1.90µm/h in dnPKA, $p <0.001$, GFP: N=3 mice, n=48 neurons, dnPKA: N=3 mice, n=146 neurons, Fig 6C movie 6, 11), increased pausing phases (76% in GFP versus 86% in dnPKA, $p<0.001$, GFP: N=3 mice, n=48 neurons, dnPKA: N=3 mice, n=146 neurons, Fig 6D) and reduced frequency of NK (3.15±0.21 NK/h in GFP versus 2.23±0.12NK/h in dnPKA, $p <0.001$, GFP: N=3 mice, n=48 neurons, dnPKA: N=3 mice, n=146 neurons, Fig 6C).

Moreover, co-transfection with centrin-RFP revealed that centrosome/nucleus coupling was also altered: the maximum distance between centrosome and nucleus during CK was reduced (GFP 12.32±0.42µm versus 10.46±0.38µm dnPKA, $p < 0.001$, GFP: N=3 mice, n=50 neurons, dnPKA: N=3 mice, n=86 neurons, Fig 6F) and the percentage of inefficient CK was increased (26% in GFP versus 37% in dnPKA, p=0.02, GFP: N=3 mice, n=50 neurons, dnPKA: N=3 mice, n=86 neurons, Fig 6G). Delocalization of PKA from the centrosome thus phenocopies cilium deletion and AC3 knock-down. This strongly suggests that centrosomal PKA is the downstream effector of the ciliary-dependent hotspot.

To further test this hypothesis, we performed a double mutation of Kif3a$^{lox/lox}$ mice by co-transfecting Cre to ablate the cilium and dnPKA to delocalize PKA. Interestingly, double mutated neurons displayed the same migratory defects as the simply mutated ones, with no additivity of the phenotypes (Fig 6C-E): speed reduction (GFP 75.49±3.48µm/h versus 55.76±1.90µm/h and 63.73±2.85 µm/h in dnPKA and CREdnPKA, $p <0.001$, GFP: N=3 mice, n=48 neurons, dnPKA: N=3 mice, n=146 neurons, CREdnPKA: N=3 mice, n=86 neurons, Fig 6C, movie 12); increased pausing phases (76% in GFP versus 86% and 84% in dnPKA and CREdnPKA, $p <0.001$, GFP: N=3 mice, n=48 neurons, dnPKA: N=3 mice, n=146 neurons, CREdnPKA: N=3 mice, n=86 neurons, Fig 6D) and reduced NK frequency (3.15±0.21 NK/h in GFP versus 2.23±0.12NK/h and 2.09±0.16NK/h in dnPKA and CREdnPKA $p <0.001$, GFP: N=3 mice, n=48 neurons, dnPKA: N=3 mice, n=146 neurons, CREdnPKA: N=3 mice, n=86 neurons, Fig 6C). The non-additivity of the migratory phenotypes strongly suggests that PKA acts downstream of the ciliary produced cAMP to regulate migration through centrosome/nucleus coupling.

The hotspot is also present in adult and embryonic migrating neurons

In order to know whether this pattern of cAMP dynamics is specific of neurons migrating tangentially in the postnatal RMS or generally used by migrating neurons, we assessed its presence in other types of neuronal migration. Postnatally generated SVZ neurons reorient radially in the OB after their tangential migration in the RMS. Ratiometric analysis of the biosensor showed that they too display a transient centrosomal hotspot (Fig 7A, movie 13). In addition, analysis of tangentially migrating neurons of the adult RMS also displayed the same hotspot (Fig 7B, movie 14). Finally, the hotspot was also present in radially migrating neurons of the embryonic cortex (Fig 7C, movie 15).

We can thus conclude that ciliary produced cAMP hospot at the centrosome is a general feature of migrating neurons.

DISCUSSION

Our work provides evidence that PC controls neuronal migration by acting on the centrosome through cAMP local diffusion. The cAMP produced by the ciliary AC3 appears as a dynamic hotspot at the centrosome present during NK, which acts on centrosomal PKA to regulate centrosome/nucleus coupling with consequences on nuclear translocation.

PC and neuronal migration

The importance of PC for neuronal migration has been inferred from ciliopathy defects (Valente et al., 2014). and evidenced in embryonic cortical interneurons (Baudoin et al., 2012; Higginbotham et al., 2012). The PC is often considered as a signaling hub and signal integrator, with paramount importance for Shh signaling (Bangs and Anderson, 2017; Baudoin et al., 2012). However, the mechanisms by which cilium-mediated signaling is converted into a migratory response are not well understood (Veland et al., 2014). Our data suggest that the PC forms a single signaling unit with the centrosome, where ciliary AC3 produces cAMP, which concentrates in the PC and diffuses to the centrosome, locally activating PKA.

The migration defects that we observe are very similar to the ones observed in cilium ablated (Baudoin et al., 2012) or Arl13B mutated migrating embryonic interneurons (Higginbotham et al., 2012). As we observed the hotspot in all types of neurons that we analyzed, one could thus imagine that the migratory defects observed in those papers might also be the consequence of a defective cAMP/PKA signaling at the centrosome.

Dynamics of the hotspot

Our discovery was made possible by the development of a challenging technique involving electroporation of neonatal mice with a sensitive FRET biosensor, coupled with spatially and temporally resolutive biphotonic imaging on acute brain sections.

cAMP signaling microdomains analyzed thanks to FRET biosensors have previously been described in different cell types. Interestingly, a study performed in Chinese Hamster Ovary cells transfected with a centrosome targeted biosensor reported a centrosomal microdomain which, contrarily to the hotspot described in our study, displayed low cAMP levels. This "coldspot" was dynamic, disappeared during mitosis and was important for cell cycle progression (Terrin et al., 2012). cAMP microdomains were also described in diverse neuronal subcompartments such as growth cones, axons and dendrites (Averaimo et al., 2016; Calebiro and Maiellaro, 2014; Castro et al., 2014). However, to our knowledge, we are the first to perform this type of analysis in migrating neurons.

We detect a surprisingly dynamic cAMP hotspot at the centrosome, cyclically present during NK and absent during pauses. We show that the PC and ciliary localized AC3 are necessary for formation of the hotspot. We thus think that the signal that we observe at the centrosome is a consequence of a short-range diffusion of the cAMP concentrated in the PC by AC3 activity. Two studies using a ciliary targeted FRET-based cAMP sensor in fibroblasts and kidney epithelial cells indeed showed that the PC is a cAMP rich microdomain (Moore et al., 2016; Sherpa et al., 2019), reaching levels of concentration as high as 5-fold higher than the rest of the cytoplasm.

The cyclical presence of the hotspot raises interesting questions. A mechanical explanation of the cyclicity could be the dynamics of the cilium itself. Two studies reported that the cilium is highly dynamic during migration of tangentially migrating embryonic neurons (Baudoin et al., 2012; Higginbotham et al., 2012) with one of them suggesting a transient disappearance of the cilium during pauses (Baudoin et al., 2012). If this is the case in RMS migrating neurons, this could explain the disappearance of the hotspot during pauses. The other possible explanation would be the cyclical regulation of AC3 either by intermittent signalization at the level of an upstream signaling receptor or by a cyclical downstream mechanism.

Centrosomal localization of PKA

PKA subcellular localization closed to its effectors is an essential determinant of cAMP signaling compartmentalization (Gervasi et al., 2007; Torres-Quesada et al., 2017) and is ensured by A Kinase Anchoring Proteins (AKAP).

In postnatal RMS migrating neurons, the catalytic sub-unit of PKA that we detected by immunoctochemistry was mainly associated with the centrosome. Such a centrosomal

localization was reported in radial glial cells (Saade et al., 2017) and lymphocyte T (Ong et al., 2018) but never in migrating neurons. RMS neurons strongly express the centrosomal AKAP pericentrin (Diviani et al., 2000; Endoh-Yamagami et al., 2010). Interestingly, RMS neurons migrating in pericentrin mutant mice devoid of PACT domain (pericentrin-AKAP450 centrosomal targeting domain) display a very similar migratory phenotype as our mutated cells. This suggests that pericentrin is the main AKAP responsible for PKA centrosomal localization in RMS cells. We used the dominant negative form of PKA described by Saade et al (Saade et al., 2017), which is a regulatory subunit of PKA devoid of the domain interacting with pericentrin. This led to efficient PKA delocalization from the centrosome and to the same migratory defects as cilium ablation and AC3 knock-down. This shows that PKA centrosomal localization through interaction with pericentrin is necessary for proper migration and that PKA is the main downstream effector of the hotspot. The subcellular co-localization of the cAMP hotspot with PKA might ensure that the concentration of the second messenger locally exceeds the activation threshold of PKA, as suggested in (Koschinski and Zaccolo, 2017).

Our data show that the activation of PKA by the ciliary produced cAMP hotspot regulates the speed of migration via centrosome/nucleus coupling. A likely PKA downstream effector could be the LIS1-dynein-nde1-ndeL1 complex, which is localized at the centrosome (Sasaki et al., 2000; Tanaka et al., 2004), essential for neuronal migration in diverse types of neurons (Bradshaw et al., 2011; Shu et al., 2004; Tsai et al., 2007) and involved in centrosome/nucleus coupling (Jheng et al., 2018; Tsai et al., 2007). PKA phosphorylates Ndel1 and Nde1, which induces the release of LIS1 and dynein from the complex (Bradshaw et al., 2011; Tsai et al., 2007) thus allowing their action on microtubule stability (Hendricks et al., 2012; Sapir, 1997). Interestingly, depletion of LIS1 induces a decrease of N-C distances and a decrease in NK frequency (Tanaka et al., 2004; Tsai et al., 2007), which is very similar to our phenotype. This suggests that impaired LIS1 release consecutive to the hotspot disappearance might be important in our phenotype. This would lead to destabilization of microtubules (Sapir, 1997) triggering a defect of microtubule tension between centrosome and nucleus (Bertipaglia et al., 2018) and leading to centrosome/nucleus coupling defects.

We thus unveil a new regulatory pathway whereby a cilium-generated signal exerts a direct action on centrosome/nucleus coupling to regulate NK. We propose that this is a generalized mode of regulation since we observed the hotspot in all migrating neurons analyzed. The existence of such a signaling unit linking PC and centrosome via cAMP could also be tested

in other ciliated cells and cellular processes involving centrosomal movements linked to microtubules remodeling.

MATERIAL AND METHODS

Mouse lines

Mice were housed in a 12-hour light/dark cycle, in cages containing 2 females and one male. The postnatal mice were housed in the cages with their parents. Animal care was conducted in accordance with standard ethical guidelines (National Institutes of Health publication no. 85-23, revised 1985 and European Committee Guidelines on the Care and Use of Laboratory Animals 86/609/EEC). The experiments were approved by the local ethics committee (Comité d'Ethique en Expérimentation Animale Charles Darwin C2EA-05 and the French Ministère de l'Education Nationale de l'Enseignement Supérieur et de la Recherche APAFIS#13624-2018021915046521_v5). We strictly performed this approved procedure. The mice used were in a C57BL6 background. Kif3a conditional knockout (Kif3a$^{lox/lox}$) (Marszalek et al., 2000) and Rpgrip1l conditional knockout (Rpgrip1l$^{lox/lox}$) were genotyped according to the original protocols.

Plasmid constructions

pCaggs-Epac-S^{H187} was derived from pCDNA3-Epac-S^{H187} kindly given by Kees Jalink (Klarenbeek et al, 2015). Minor modification on the Epac-S^{H187} sequence was performed to reduce redundancy. pCaggs-GFP, pCaggs-CRE-IRES-GFP and pCaggs-CRE-IRES-Tdtomato were designed in the laboratory. pCIG-PKA RIΔ2-6 wt subunit flagged (call later on pdn-PKA) was kindly given by Elisa Marti (Saade et al, 2017). pCs2-Centrin-RFP was ordered in addgene (#26753). All the plasmids were used at a concentration between 5 to 8µg/µL (0,01% Fast green) for postnatal electroporation, 2µg/µL (0,01% Fast green) for in utero electroporation and 10µg/µL for adult electroporation.

miRNA production

Silencing of AC3 has been performed using BLOCK-iT™ Pol II miR RNAi Expression Vector kits (Invitrogen) and the RNAi Designer (Invitrogen). The sequence of the single stranded oligos are AC3.3: top: TGCTGTTAGGATGGAGCACACGGCATGTTTTG GCCACTGACTGACATGCCGTGCTCCATCCTAA, bottom: CCTGTTAGGATGGAGCA CGGCATGTCAGTCAGTGGCCAAAACATGCCGTGTGCTCCATCCTAAC. The double stranded oligos were inserted in a pcDNA™6.2-GW/EmGFP-miR. To produce the pcDNA™6.2-GW/Tdtomato-miR, GFP was replaced by tdTomato using Dra1 and BamHI. The resulting constructions were sequenced before use.
To validate the AC3 miRNAs, NIH3T3 cells were co-transfected with a plasmid over-expressing AC3 and either miRAC3 or the negative control miRneg. 48h post-transfection, the total RNAs were extracted with kit NucleoSpin RNA (ref: 740955.50, Macherey-Nagel) and used as template for reverse transcription with Maxima reverse transcriptase and random hexamers (Fermentas, Thermo Fisher Scientific). The resulting cDNAs were amplified by quantitative PCR performed in the Lightcycler 480 detection system (Roche) using the LC480 SYBR green I Master mix (Roche). The results were analyzed with the LC480 Software (Roche) to assess the relative quantities of AC3 mRNAs. The AC3 primers were: forward: AAGGACCAGCAGCAGTTCAATA; reverse: ATCCTC GTGGTGGTATTTGG. The B2M and PPIA reference genes were selected among the Mouse SYBR reference gene panel (Tataabiocenter) with the NormFinder software (Andersen et al., 2004).

Postnatal electroporation

Postnatal electroporation was performed at P2. The postnatal mice were anesthetized by hypothermia. Pseudo-stereotaxic injection (from lambda ML: -1,2, A/P:2, D/V: 2,5-2) using glass micropipette (Drummond scientific company, wiretol I 50µL, 5-000-1050) was performed and 2µL of plasmid (betweeen 5 and 8 µg/µL) were injected. Animals were subjected to 5 pulses of 99,99V during 50ms separated by 950ms using the CUY21 SC Electroporator and 10mm tweezer electrode (CUY650-10 Nepagene). The animals were placed on 37°C plates to restore their body temperature before returning with their mother. Animals were considered as fully restored when pups were moving naturally, and their skin color returned to pink.

Acute brain slices

Brain slices from mice aged from P6 to P10 were prepared as previously described (Castro et al., 2010). Pups were killed by decapitation and the brain was quickly removed from the skull. 250µm sagittal brain slices were cut with a VT1200S microtome (Leica). Slices were prepared in the ice-cold cutting solution of the following composition: 125mM NaCl, 0.4mM $CaCl_2$, 1mM $MgCl_2$, 1.25mM NaH_2PO_4, 26mM $NaHCO_3$, 5mM sodium pyruvate, 20mM glucose and 1mM kynurenic acid, saturated with 5% CO_2 and 95% O_2. Slices were incubated in this solution for 30 min at room temperature and then placed in recording solution (identical to the solution used for cutting, except that the Ca^{2+} concentration was 2mM and kynurenic acid was absent) for at least 30 min at 32°C before image acquisition.

Time-lapse video microscopy

To analyze cell migration and centrosome dynamics, images were obtained with an inverted SP5D confocal microscope (Leica). Images were taken every 3 min for 2-3h using a 40X/ 1,25 N.A. objective with 1.5 optical zoom.

Biosensor images were acquired with an upright multiphoton microscope Leica SP5 MPII with a 25x/ 0,95 N.A, objective, 4x optical zoom, and GaAsP hybrid detector. The excitation wavelength was set at 850 nm to excite the the mTurquoise2 donor. The two emission wavelengths were acquired simultaneously with filters of 479+/-40 nm and 540+/-50 nm. Image stacks with 2µm intervals were taken every minute for 1h. The presence of tdTomato, indicative of CRE recombinase or miRNA, was assessed with a confocal head before and after the movies. For codetection of the centrin-RFP and biosensor, two-photon excitation for the biosensor and confocal headfor centrin-RFP were used alternatively. Stacks were spaced by 1µm and acquired every 2 minutes.

The temperature in the microscope chamber was maintained at 32°C, for embryos and postnatal imaging, or 35°C, for P30 imaging, and brain slices were continuously perfused with heated recording solution (see above) saturated with 5% CO_2 and 95% O_2

Analyses of neuronal migration

Analyses were performed using ImageJ (NIH Image; National Institutes of Health, Bethesda, MD) software and MTrackJ plugging (Meijering et al., 2012). The nucleus and the centrosome of each cell were tracked manually on each time frame during the whole movie.

For cell migration and centrosome movement characteristics, calculation of speed, nuclear translocation frequency and pausing time were performed using the x,y,t coordinates of the nucleus of each cell.

Cells were excluded from the analysis if they were tracked during less than 30 min or did not perform any nuclear translocation during the whole tracking. A cell was considered as migrating if it performed a distance superior to 6 µm during a 3-minute interval.

A centrokinesis was defined as a forward movement superior to 2 µm followed by a backward movement superior to 2 µm. Maximal distance between centrosome and nucleus of every centrokinesis was considered.

Quantification of biosensor images

Image stacks obtained for donor and acceptor emission were processed with a custom code developed in the IGOR Pro environment (Wavemetrics, Lake Oswego, OR, USA). The maximum intensity was projected vertically to form a 2D image. The fluorescence intensity of donor and acceptor were averaged to build an image indicating biosensor concentration. The fluorescence intensity of donor and acceptor were ratioed for each pixel to report biosensor activation level. For each experiment, ratio values were multiplied by a constant such that baseline ratio was 1. These images were combined to produce pseudocolor images, with the ratio used as hue (from blue to red) and the intensity as value, while the saturation was set to the maximum (Polito et al., 2014; Tsien and Harootunian, 1990).

For each migrating neuron, the ratio was then measured along its migration direction, calculated as follows. A series of anchor points were manually positioned along the length of the cell, and the profile of ratio and intensity was calculated along these line segments, over a total width of 1 µm. The intensity profile was annotated manually, marking the rear of the cell and the tip of the leading process of the migrating neuron, and both sides of the nucleus. The movement of the nucleus was then used to determine the orientation of the migration, by fitting a line to the positions of the nucleus for all time points. Coordinates in the frame of reference of the image were then converted to a single position along the axis of cell migration.

Immunohistochemistry

P7-P10 mice were lethally anesthetized using euthasol. Intracardiac perfusion with 4% paraformaldehyde were performed. Brain were postfixed overnight in 4% paraformaldehyde.

Three rinses were done with PBS 1x (gibco 1400-067). 50µm sagittal slices were cut with VT1200S microtome (Leica). Slices were placed one hour in a saturation solution (10% fetal bovine serum; 0,5% Triton-X in PBS). The primary antibodies used in this study were: GFP (Aves, GFP-1020, 1/1000), PKAc (Cell Signaling Technology, #4782 1/250), AC3 (Santa Cruz, C-20 sc-588, 1/200), Arl13b (UC Davis/NIH NeuroMab Facility, 75-287, 1/1000), ɣ-tubulin (Sigma-Aldrich, T6557, 1/500). The antibodies were diluted in saturation solution. Slices were incubated 48 to 72h at 4°C under agitation with the antibodies. Three rinses were done with PBS 1x. The secondary antibodies used were: anti-chicken IgY alexa Fluor 488 (1/1000, Jackson ImmunoResearch: 703-545-155) against anti-GFP, anti-rabbit IgG Cy5 (1/1000, Jackson ImmunoResearch: 711-175-152) against anti-PKAc, anti-rabbit IgG Cy3 (1/2000, Jackson ImmunoResearch: 711-165-152) against anti-AC3, anti-Mouse IgG, Fcɣ Subclass 1 specific alexa Fluor 594 (1/2000, Jackson ImmunoResearch: 115-585-205) against anti-ɣ-tubulin, anti-Mouse IgG, Fcɣ subclass 2a specific alexa Fluor 647 (1/1000, Jackson ImmunoResearch: 115-605-206) against anti-Arl13b . The antibodies were diluted in saturation solution. Slices were incubated 1h at room temperature under agitation with the secondary antibody solution. Three rinses with PBS 1X were done. Slices were counter-colored with Hoeschst and mounted with Mowiol.

Statistics

All manipulations and statistical analyses were implemented with R (3.5.1). Normality in the variable distributions was assessed by the Shapiro-Wilk test. Furthermore, the Levene test was performed to probe homogeneity of variances across groups. Variables that failed the Shapiro-Wilk or the Levene test were analyzed with nonparametric statistics using the one-way Kruskal–Wallis analysis of variance on ranks followed by Nemenyi test post hoc and Mann–Whitney rank sum tests for pair-wise multiple comparisons. Variables that passed the normality test were analyzed by means of one-way ANOVA followed by Tukey post hoc test for multiple comparisons or by Student's t test for comparing two groups. Categorical variables were compared using Pearson's Chi-squared test or Fisher's exact test. All the statistical analyses have been performed on the five groups together (GFP, Cre, miRAC3, dnPKA, dnPKA/CRE).

A p value of < 0.05 was used as a cutoff for statistical significance. Results are presented as the mean ± SD or medians and the given values in the text are the mean ± SEM, unless otherwise stated. The statistical tests are described in each figure legend.

Acknowledgments

We thank Sylvie Schneider-Maunoury for Rpgrip1l mice. We are grateful to Kees Jalink for Epac SH187 plasmid and to Elisa Marti for dnPKA plasmid. Nathalie Spassky and Alice Meunier gave us AC3 antibodies. The experiments were performed in IBPS imaging facility and the mice were housed in IBPS animal facility. We thank Claire Fournier-Thibault for lending her electroporator. We are grateful to all re-readers and especially Isabelle Dusart. This work was supported by CNRS, INSERM, Fondation Lejeune and Sorbonne University. JS was funded by a doctoral fellowship awarded by IBPS to AT and PV labs. This work was supported (in part) by the Investissements d'Avenir program managed by the ANR under reference ANR-11-IDEX-0004-02. AT and PV labs are members of the Bio-Psy Labex.

REFERENCES

Andersen, C.L., Jensen, J.L., and Ørntoft, T.F. (2004). Normalization of Real-Time Quantitative Reverse Transcription-PCR Data: A Model-Based Variance Estimation Approach to Identify Genes Suited for Normalization, Applied to Bladder and Colon Cancer Data Sets. Cell Tumor Biol.

Arts, H.H., Doherty, D., van Beersum, S.E.C., Parisi, M.A., Letteboer, S.J.F., Gorden, N.T., Peters, T.A., Märker, T., Voesenek, K., Kartono, A., et al. (2007). Mutations in the gene encoding the basal body protein RPGRIP1L, a nephrocystin-4 interactor, cause Joubert syndrome. Nat. Genet. *39*, 882–888.

Averaimo, S., Assali, A., Ros, O., Couvet, S., Zagar, Y., Genescu, I., Rebsam, A., and Nicol, X. (2016). A plasma membrane microdomain compartmentalizes ephrin-generated cAMP signals to prune developing retinal axon arbors. Nat. Commun. *7*, 12896.

Bangs, F., and Anderson, K.V. (2017). Primary Cilia and Mammalian Hedgehog Signaling. Cold Spring Harb. Perspect. Biol. *9*, a028175.

Baudoin, J.-P., Viou, L., Launay, P.-S., Luccardini, C., Espeso Gil, S., Kiyasova, V., Irinopoulou, T., Alvarez, C., Rio, J.-P., Boudier, T., et al. (2012). Tangentially Migrating Neurons Assemble a Primary Cilium that Promotes Their Reorientation to the Cortical Plate. Neuron *76*, 1108–1122.

Bellion, A., Baudoin, J.-P., Alvarez, C., Bornens, M., and Métin, C. (2005). Nucleokinesis in Tangentially Migrating Neurons Comprises Two Alternating Phases: Forward Migration of the Golgi/Centrosome Associated with Centrosome Splitting and Myosin Contraction at the Rear. J. Neurosci. *25*, 5691–5699.

Belvindrah, R., Natarajan, K., Shabajee, P., Bruel-Jungerman, E., Bernard, J., Goutierre, M., Moutkine, I., Jaglin, X.H., Savariradjane, M., Irinopoulou, T., et al. (2017). Mutation of the α-tubulin Tuba1a leads to straighter microtubules and perturbs neuronal migration. J. Cell Biol. *216*, 2443–2461.

Bertipaglia, C., Gonçalves, J.C., and Vallee, R.B. (2018). Nuclear migration in mammalian

brain development. Semin. Cell Dev. Biol. *82*, 57–66.

Bishop, G.A., Berbari, N.F., Lewis, J., and Mykytyn, K. (2007). Type III adenylyl cyclase localizes to primary cilia throughout the adult mouse brain. J. Comp. Neurol. *505*, 562–571.

Bradshaw, N.J., Soares, D.C., Carlyle, B.C., Ogawa, F., Davidson-Smith, H., Christie, S., Mackie, S., Thomson, P.A., Porteous, D.J., and Millar, J.K. (2011). PKA Phosphorylation of NDE1 Is DISC1/PDE4 Dependent and Modulates Its Interaction with LIS1 and NDEL1. J. Neurosci. *31*, 9043–9054.

Calebiro, D., and Maiellaro, I. (2014). cAMP signaling microdomains and their observation by optical methods. Front. Cell. Neurosci. *8*.

Castro, L.R.V., Gervasi, N., Guiot, E., Cavellini, L., Nikolaev, V.O., Paupardin-Tritsch, D., and Vincent, P. (2010). Type 4 Phosphodiesterase Plays Different Integrating Roles in Different Cellular Domains in Pyramidal Cortical Neurons. J. Neurosci. *30*, 6143–6151.

Castro, L.R.V., Guiot, E., Polito, M., Paupardin-Tritsch, D., and Vincent, P. (2014). Decoding spatial and temporal features of neuronal cAMP/PKA signaling with FRET biosensors. Biotechnol. J. *9*, 192–202.

Diviani, D., Langeberg, L.K., Doxsey, S.J., and Scott, J.D. (2000). Pericentrin anchors protein kinase A at the centrosome through a newly identified RII-binding domain. Curr. Biol. *10*, 417–420.

Endoh-Yamagami, S., Karkar, K.M., May, S.R., Cobos, I., Thwin, M.T., Long, J.E., Ashique, A.M., Zarbalis, K., Rubenstein, J.L.R., and Peterson, A.S. (2010). A mutation in the pericentrin gene causes abnormal interneuron migration to the olfactory bulb in mice. Dev. Biol. *340*, 41–53.

Gervasi, N., Hepp, R., Tricoire, L., Zhang, J., Lambolez, B., Paupardin-Tritsch, D., and Vincent, P. (2007). Dynamics of Protein Kinase A Signaling at the Membrane, in the Cytosol, and in the Nucleus of Neurons in Mouse Brain Slices. J. Neurosci. *27*, 2744–2750.

Guo, J., Higginbotham, H., Li, J., Nichols, J., Hirt, J., Ghukasyan, V., and Anton, E.S. (2015). Developmental disruptions underlying brain abnormalities in ciliopathies. Nat. Commun. *6*, 7857.

Haase, A. (2003). Nitric oxide and cyclic nucleotides are regulators of neuronal migration in an insect embryo. Development *130*, 3977–3987.

Hendricks, A.G., Lazarus, J.E., Perlson, E., Gardner, M.K., Odde, D.J., Goldman, Y.E., and Holzbaur, E.L.F. (2012). Dynein Tethers and Stabilizes Dynamic Microtubule Plus Ends. Curr. Biol. *22*, 632–637.

Higginbotham, H., Eom, T.-Y., Mariani, L.E., Bachleda, A., Hirt, J., Gukassyan, V., Cusack, C.L., Lai, C., Caspary, T., and Anton, E.S. (2012). Arl13b in Primary Cilia Regulates the Migration and Placement of Interneurons in the Developing Cerebral Cortex. Dev. Cell *23*, 925–938.

Hildebrandt, F., Benzing, T., and Katsanis, N. (2011). Ciliopathies. N. Engl. J. Med. *364*, 1533–1543.

Howe, A.K. (2011). Cross-talk between calcium and protein kinase A in the regulation of cell

migration. Curr. Opin. Cell Biol. *23*, 554–561.

Howe, A.K., Baldor, L.C., and Hogan, B.P. (2005). Spatial regulation of the cAMP-dependent protein kinase during chemotactic cell migration. Proc. Natl. Acad. Sci. *102*, 14320–14325.

Jheng, G.-W., Hur, S.S., Chang, C.-M., Wu, C.-C., Cheng, J.-S., Lee, H.-H., Chung, B.-C., Wang, Y.-K., Lin, K.-H., del Álamo, J.C., et al. (2018). Lis1 dysfunction leads to traction force reduction and cytoskeletal disorganization during cell migration. Biochem. Biophys. Res. Commun. *497*, 869–875.

Juric-Sekhar, G., Adkins, J., Doherty, D., and Hevner, R.F. (2012). Joubert syndrome: brain and spinal cord malformations in genotyped cases and implications for neurodevelopmental functions of primary cilia. Acta Neuropathol. (Berl.) *123*, 695–709.

Klarenbeek, J., Goedhart, J., van Batenburg, A., Groenewald, D., and Jalink, K. (2015). Fourth-generation epac-based FRET sensors for cAMP feature exceptional brightness, photostability and dynamic range: characterization of dedicated sensors for FLIM, for ratiometry and with high affinity. PloS One *10*, e0122513.

Koschinski, A., and Zaccolo, M. (2017). Activation of PKA in cell requires higher concentration of cAMP than in vitro: implications for compartmentalization of cAMP signalling. Sci. Rep. *7*, 14090.

Lefkimmiatis, K., and Zaccolo, M. (2014). cAMP signaling in subcellular compartments. Pharmacol. Ther. *143*, 295–304.

Lois, C., and Alvarez-BuyIIa, A. (1994). To investigate whether SVZ cells from adult mice could differentiate into neurons. *264*, 5.

Lois, C., Garc a-Verdugo, J.-M., and Alvarez-Buylla, A. (1996). Chain Migration of Neuronal Precursors. Science *271*, 978–981.

Maiellaro, I., Lohse, M.J., Kittel, R.J., and Calebiro, D. (2016). cAMP Signals in Drosophila Motor Neurons Are Confined to Single Synaptic Boutons. Cell Rep. *17*, 1238–1246.

Mandl, L., and Megele, R. (1989). Primary cilia in normal human neocortical neurons. Z Mikrosk Anat Forsch.

Marszalek, J.R., Liu, X., Roberts, E.A., Chui, D., Marth, J.D., Williams, D.S., and Goldstein, L.S.B. (2000). Genetic Evidence for Selective Transport of Opsin and Arrestin by Kinesin-II in Mammalian Photoreceptors. Cell *102*, 175–187.

Meijering, E., Dzyubachyk, O., and Smal, I. (2012). Methods for Cell and Particle Tracking. In Methods in Enzymology, (Elsevier), pp. 183–200.

Moore, B.S., Stepanchick, A.N., Tewson, P.H., Hartle, C.M., Zhang, J., Quinn, A.M., Hughes, T.E., and Mirshahi, T. (2016). Cilia have high cAMP levels that are inhibited by Sonic Hedgehog-regulated calcium dynamics. Proc. Natl. Acad. Sci. *113*, 13069–13074.

Ong, S.T., Chalasani, M.L.S., Fazil, M.H.U.T., Prasannan, P., Kizhakeyil, A., Wright, G.D., Kelleher, D., and Verma, N.K. (2018). Centrosome- and Golgi-Localized Protein Kinase N-Associated Protein Serves As a Docking Platform for Protein Kinase A Signaling and Microtubule Nucleation in Migrating T-Cells. Front. Immunol. *9*, 397.

Patel, S., and Barkovich, A.J. (2002). Analysis and Classification of Cerebellar Malformations. 14.

Polito, M., Vincent, P., and Guiot, E. (2014). Biosensor imaging in brain slice preparations. Methods Mol Biol.

Quiquempoix, M., Fayad, S.L., Boutourlinsky, K., Leresche, N., Lambert, R.C., and Bessaih, T. (2018). Layer 2/3 Pyramidal Neurons Control the Gain of Cortical Output. Cell Rep. *24*, 2799-2807.e4.

Rosenbaum, J.L., and Witman, G.B. (2002). Intraflagellar transport. Nat. Rev. Mol. Cell Biol. *3*, 813–825.

Saade, M., Gonzalez-Gobartt, E., Escalona, R., Usieto, S., and Martí, E. (2017). Shh-mediated centrosomal recruitment of PKA promotes symmetric proliferative neuroepithelial cell division. Nat. Cell Biol. *19*, 493–503.

Sapir, T. (1997). Reduction of microtubule catastrophe events by LIS1, platelet-activating factor acetylhydrolase subunit. EMBO J. *16*, 6977–6984.

Sasaki, S., Shionoya, A., Ishida, M., Gambello, M.J., Yingling, J., Wynshaw-Boris, A., and Hirotsune, S. (2000). A LIS1/NUDEL/Cytoplasmic Dynein Heavy Chain Complex in the Developing and Adult Nervous System. Neuron *28*, 681–696.

Schaar, B.T., and McConnell, S.K. (2005). Cytoskeletal coordination during neuronal migration. Proc. Natl. Acad. Sci. U. S. A. *102*, 13652–13657.

Sherpa, R.T., Mohieldin, A.M., Pala, R., Wachten, D., Ostrom, R.S., and Nauli, S.M. (2019). Sensory primary cilium is a responsive cAMP microdomain in renal epithelia. Sci. Rep. *9*, 6523.

Shu, T., Ayala, R., Nguyen, M.-D., Xie, Z., Gleeson, J.G., and Tsai, L.-H. (2004). Ndel1 Operates in a Common Pathway with LIS1 and Cytoplasmic Dynein to Regulate Cortical Neuronal Positioning. Neuron *44*, 263–277.

Silva, C.G., Peyre, E., and Nguyen, L. (2019). Cell migration promotes dynamic cellular interactions to control cerebral cortex morphogenesis. 12.

Tanaka, T., Serneo, F.F., Higgins, C., Gambello, M.J., Wynshaw-Boris, A., and Gleeson, J.G. (2004). Lis1 and doublecortin function with dynein to mediate coupling of the nucleus to the centrosome in neuronal migration. J. Cell Biol. *165*, 709–721.

Terrin, A., Monterisi, S., Stangherlin, A., Zoccarato, A., Koschinski, A., Surdo, N.C., Mongillo, M., Sawa, A., Jordanides, N.E., Mountford, J.C., et al. (2012). PKA and PDE4D3 anchoring to AKAP9 provides distinct regulation of cAMP signals at the centrosome. J. Cell Biol. *198*, 607–621.

Tobin, J.L., Di Franco, M., Eichers, E., May-Simera, H., Garcia, M., Yan, J., Quinlan, R., Justice, M.J., Hennekam, R.C., Briscoe, J., et al. (2008). Inhibition of neural crest migration underlies craniofacial dysmorphology and Hirschsprung's disease in Bardet-Biedl syndrome. Proc. Natl. Acad. Sci. *105*, 6714–6719.

Toriyama, M., Mizuno, N., Fukami, T., Iguchi, T., Toriyama, M., Tago, K., and Itoh, H. (2012). Phosphorylation of Doublecortin by Protein Kinase A Orchestrates Microtubule and

Actin Dynamics to Promote Neuronal Progenitor Cell Migration. J. Biol. Chem. *287*, 12691–12702.

Torres-Quesada, O., Mayrhofer, J.E., and Stefan, E. (2017). The many faces of compartmentalized PKA signalosomes. Cell. Signal. *37*, 1–11.

Tsai, J.-W., Bremner, K.H., and Vallee, R.B. (2007). Dual subcellular roles for LIS1 and dynein in radial neuronal migration in live brain tissue. Nat. Neurosci. *10*, 970–979.

Tsien, R.Y., and Harootunian, A.T. (1990). Practical design criteria for a dynamic ratio imaging system. Cell Calcium *11*, 93–109.

Valente, E.M., Rosti, R.O., Gibbs, E., and Gleeson, J.G. (2014). Primary cilia in neurodevelopmental disorders. Nat. Rev. Neurol. *10*, 27–36.

Veland, I.R., Lindb\a ek, L., and Christensen, S.T. (2014). Linking the primary cilium to cell migration in tissue repair and brain development. Bioscience *64*, 1115–1125.

Wichterle, H., García-Verdugo, J.M., and Alvarez-Buylla, A. (1997). Direct Evidence for Homotypic, Glia-Independent Neuronal Migration. Neuron *18*, 779–791.

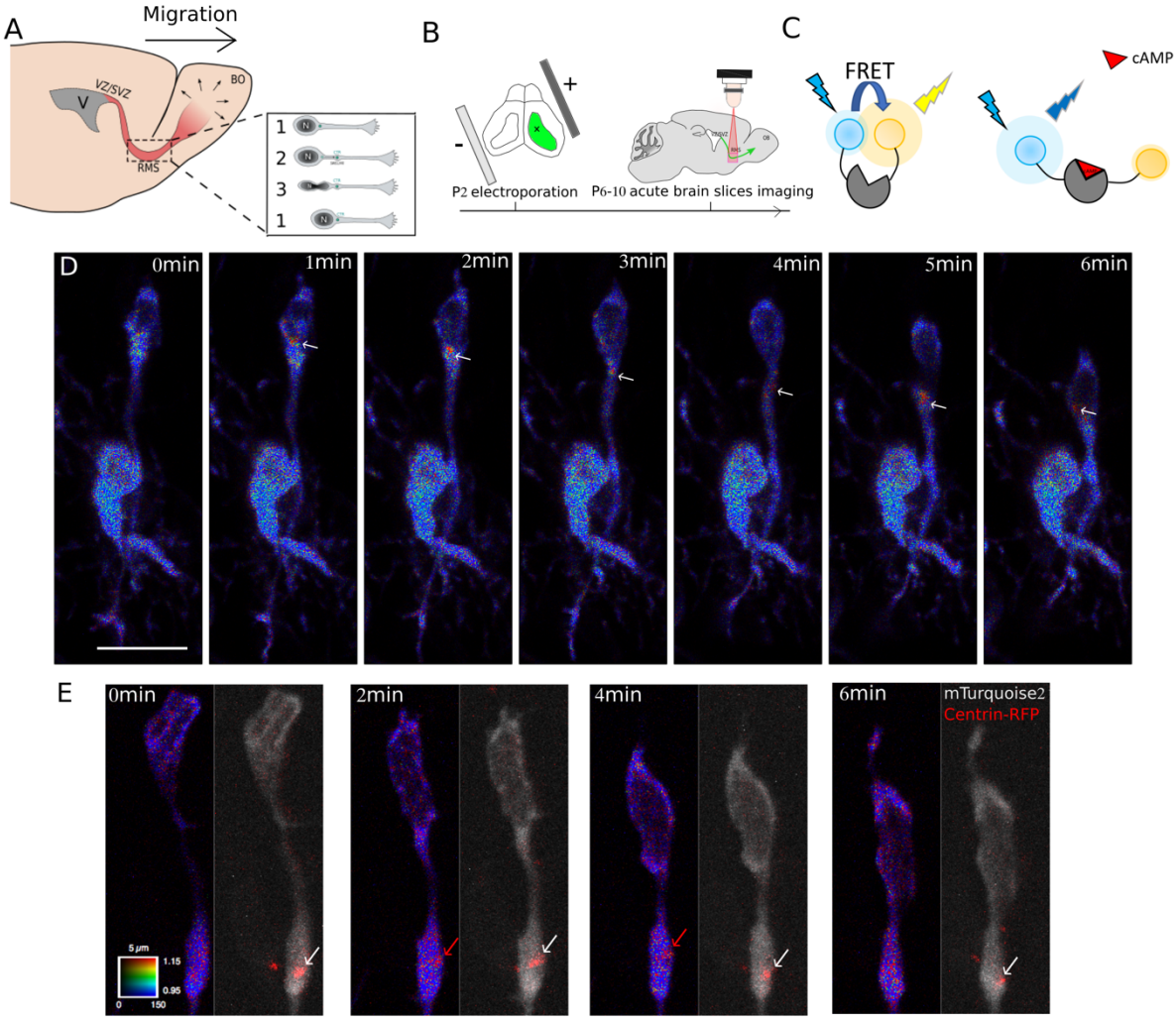

Figure 1: **cAMP dynamics in migrating neurons of the mouse postnatal RMS**

A) Scheme of SVZ-OB migration pathway and of cyclic saltatory migration.
1: pausing phase. 2: extension of the leading process and centrosome forward movement into a swelling ahead of the nucleus. 3: nucleokinesis with the nucleus moving towards the centrosome. 1: pause at a forward position.

B) Scheme of the postnatal experimental procedure.

C) The Epac-S^{H187} biosensor cAMP is composed of a part of Epac protein coupled to a donor and an acceptor fluorophore. It switches from a low FRET conformation to a higher FRET conformation upon binding of cAMP (red triangle). Changes in cAMP concentration are analyzed by ratio-ing donor (cyan, mTurquoise2) and acceptor (yellow, td-cpVenus) images, and represented by false colors as in D.

D) Live two-photon imaging of a representative migrating neuron transfected by Epac-S^{H187}. The white arrows show a dynamic cAMP hotspot present during NK. A non-migrating transfected cell is present in the field of view. Scale bar 10µm

E) Live biphotonic and confocal imaging of a representative migrating neuron transfected by Epac-S^{H187} and Centrin-RFP. The white arrows show a dynamic cAMP hotspot present during NK at the centrosome. The centrin-RFP and biosensor signals in the 4min images appear slighly shifted. This is likely due to the 1-minute interval between the two signal acquisitions.

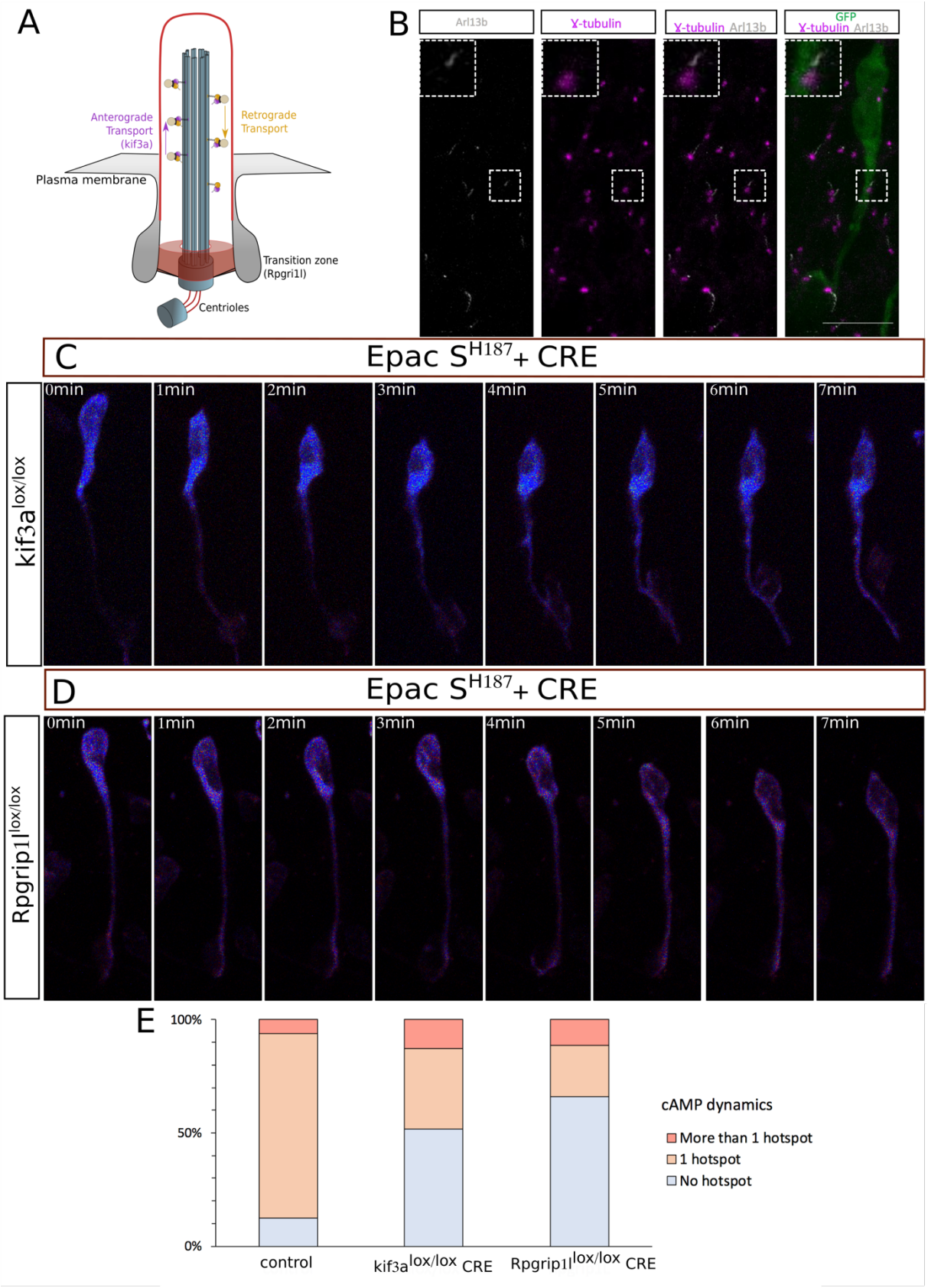

Figure 2: **Primary cilium ablation leads to disappearance of the cAMP hotspot in the majority of neurons.**

A) Scheme of a primary cilium.

B) Immunohistochemistry of a GFP positive RMS neuron showing a short Arl13b positive primary cilium (gray) connected to the ɣ-tubulin positive centrosome (magenta). Scale bar 10 µm

C) Live biphotonic imaging of a representative migrating neuron transfected by Epac-S^{H187} and Cre recombinase in a $Kif3a^{lox/lox}$ mouse. The cAMP hotspot is not detected.

D) Live biphotonic imaging of a representative migrating neuron transfected by Epac-S^{H187} and Cre recombinase in a $Rpgrip1l^{lox/lox}$ mouse. The cAMP hotspot is not detected.

E) Percentage of neurons with no hotspot, one or more than one hotspot in control or $Kif3a^{lox/lox}$ and $Rpgrip1^{lox/lox}$ CRE transfected migrating neurons. (control: N=10 mice, n=101 cells, Kif3a: N= 4, n=36, Rpgrip1l: N=5, n=52). (Fisher's Exact Test for Count Data, $p < 0.001$)

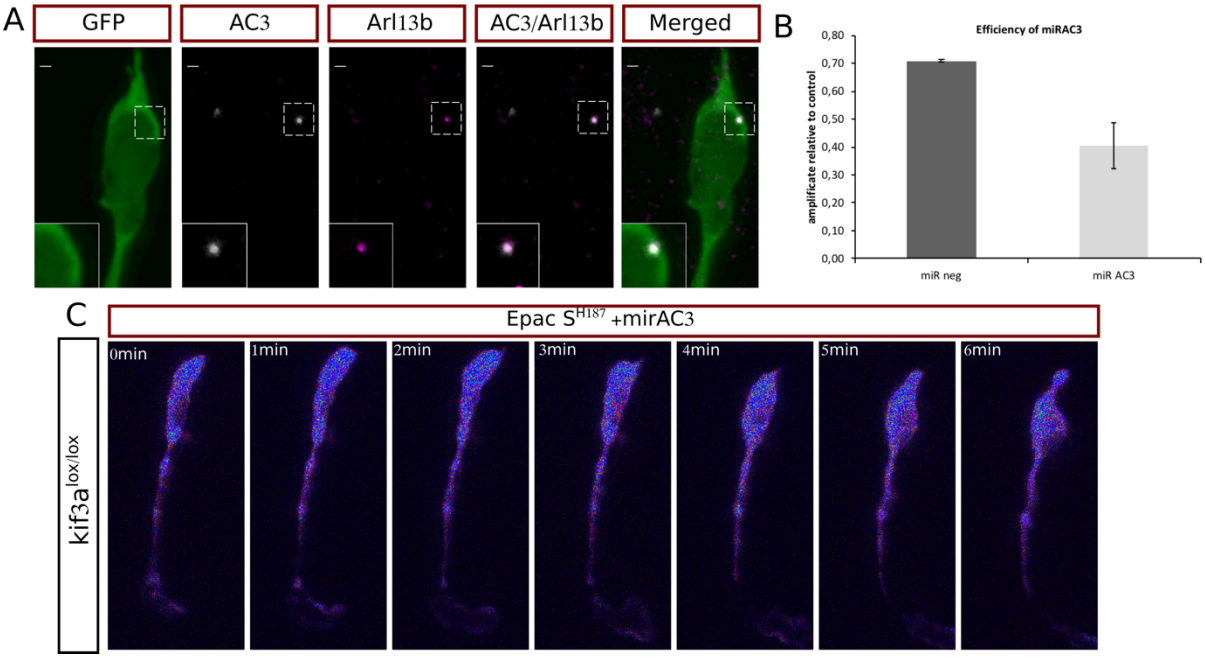

Figure 3: **Ciliary AC3 deletion leads to disappearance of the cAMP hotspot**

A) Immunocytochemistry of a GFP positive RMS neuron showing AC3 subcellular localization (magenta) in the Arl13B positive primary cilium (gray). Scale bar 1 µm

B) Histogram representing the efficacy of the miRAC3 observed by RT qPCR.

C) Live biphotonic imaging of a representative migrating neuron transfected by Epac-S^{H187} and miRAC3. The cAMP hotspot is not detected.

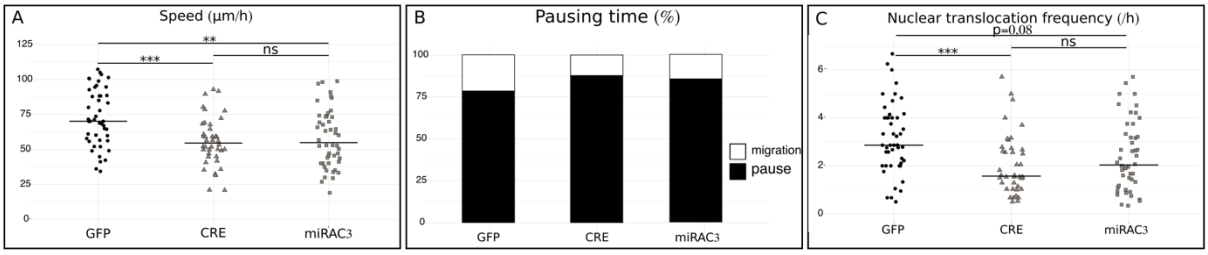

Figure 4: **Migration defects after primary cilium ablation and AC3 knock-down**

A) Average speed of neurons electroporated with GFP, CRE-GFP or miRAC3-GFP in Kif3a$^{lox/lox}$ background. The black line represents the median. (one way anova($F_{(4,346)}$=7.94, $p < 0.001$, followed by Tukey HSD test (* $p < 0.05$, *** $p < 0.001$), GFP: N=3, n=48, CRE: N=3, n=40, miRAC3: N=2, n=48)

B) Percentage of pausing time of neurons electroporated with GFP, CRE-GFP or miRAC3-GFP in Kif3a$^{lox/lox}$ background. (GFP: N=3, n=48, CRE: N=3, n=40, miRAC3: N=2, n=48) (Pearson's Chi-squared test X^2= 40.032, p-value < 0.001)

C) NK frequency of neurons electroporated with GFP, CRE-GFP or miRAC3-GFP in Kif3a$^{lox/lox}$ background. The black line represents the median. (One-way Kruskal-Wallis test (Chi square X^2= 19.79, $p < 0.001$, df = 4, followed by Nemenyi test (* $p < 0.05$, *** $p < 0.001$), GFP: N=3, n=48, CRE: N=3, n=40, miRNA-AC3: N=2, n=48)

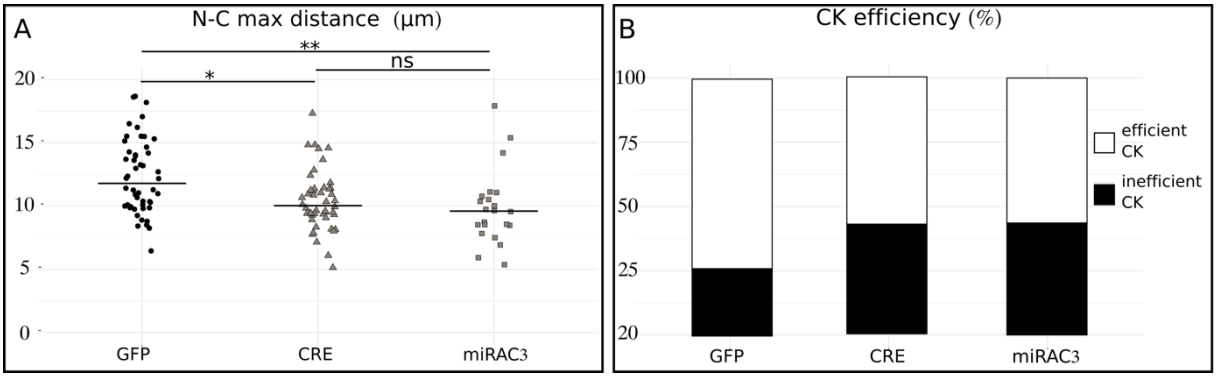

Figure 5: **Centrosome-nucleus coupling defects after primary cilium and AC3 knock-down ablation**

A) Maximal distance between nucleus and centrosome during CK of neurons electroporated with centrin-RFP and GFP, CRE-GFP or miRAC3-GFP in Kif3a$^{lox/lox}$ background. The black line represents the median. (One-way Kruskal-Wallis test (Chi square X^2= 8.11, $p < 0.001$, df = 3, followed by Nemenyi test (* $p < 0.05$, ** $p < 0.01$), GFP: N=3, n=50, CRE: N=3, n=46, miRAC3: N=2, n=22)

B) Percentage of CK efficiency in neurons electroporated with centrin-RFP and GFP, CRE-GFP or miRAC3-GFP in Kif3a$^{lox/lox}$ background. (Pearson's Chi-squared test X^2= 12.23, p-value =0.002), GFP: N=3 mice, n=48 neurons, CRE: N=3 mice, n=40 neurons, miRAC3: N=2 mice, n=48 neurons)

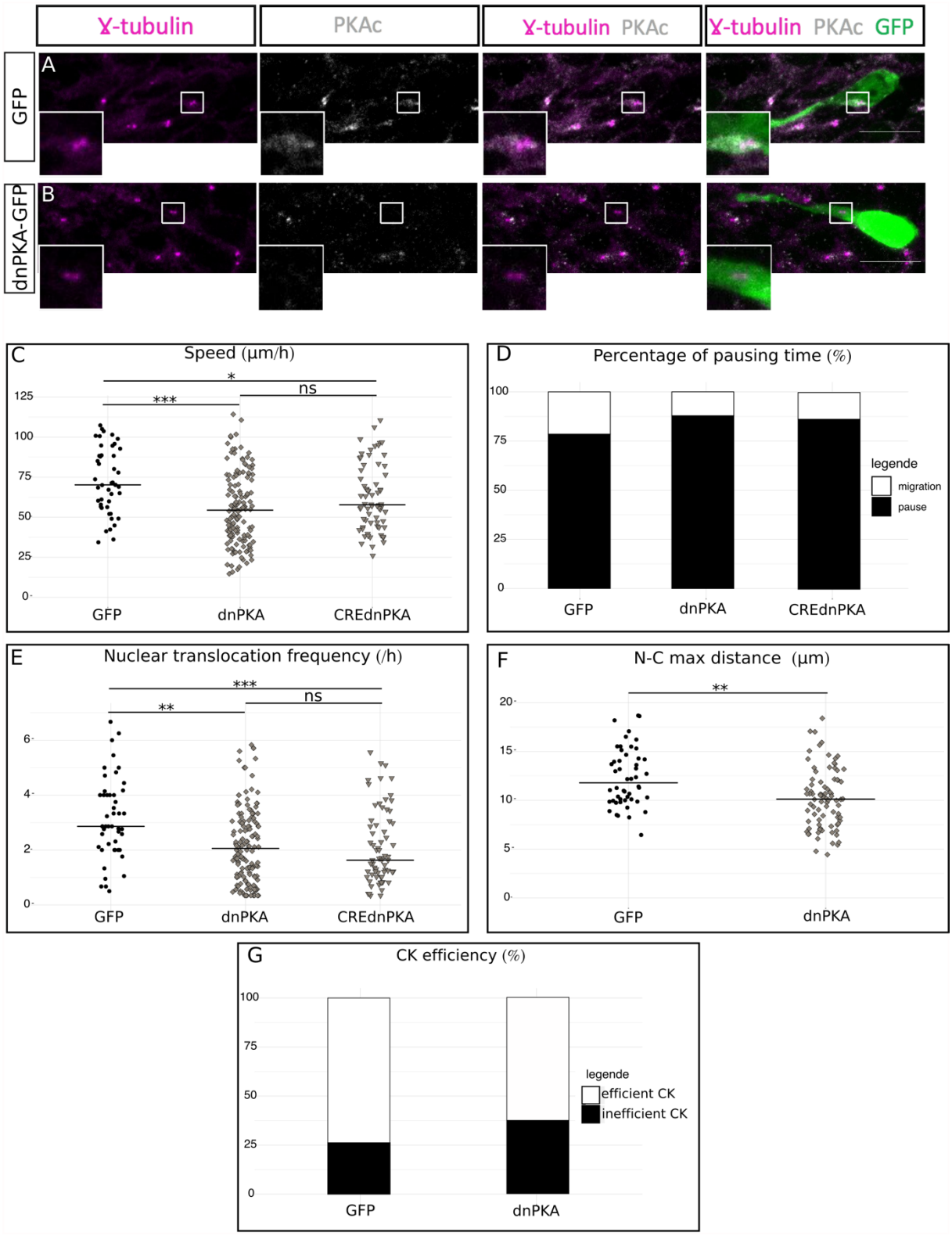

Figure 6: **PKA is centrosomal and its delocalization phenocopies cilium ablation**

A) Immunocytochemistry of a GFP positive RMS neuron showing PKAc subcellular localization (grey) around ɣ-tubulin positive centrosome (magenta). Scale bar 10 µm

B) Immunocytochemistry of a dnPKA-GFP positive RMS neuron showing a delocalisation of PKAc subcellular localization (grey). ɣ-tubulin labelled the centrosome (magenta). Scale bar 10 µm.

C) Average speed of neurons electroporated with GFP, dnPKA-GFP or dnPKA-GFP plus CRE-TdTomato in Kif3a$^{lox/lox}$ background. The black line represents the median. (one way anova($F_{(4,346)}$=7.94, $p < 0.001$, followed by Tukey HSD test (* $p < 0.05$, *** $p < 0.001$), GFP: N=3, n=48, dnPKA: N=3, n=146, CREdnPKA: N=3, n=86)

D) Percentage of pausing time of neurons electroporated with GFP, dnPKA-GFP or dnPKA-GFP/CRE-TdTomato in Kif3a$^{lox/lox}$ background. The black line represents the median.(GFP: N=3, n=48, dnPKA: N=3, n=146, CREdnPKA: N=3, n=86). (Pearson's Chi-squared test X^2= 67.25, p-value < 0.001)

E) Nuclear translocation frequency of neurons electroporated with GFP, dnPKA-GFP or dnPKA-GFP/CRE-TdTomato in Kif3a$^{lox/lox}$ background. The black line represents the median. (One-way Kruskal-Wallis test (Chi square X^2= 19.79, $p < 0.001$, df = 4, followed by Nemenyi test (* $p < 0.05$, *** $p < 0.001$), GFP: N=3, n=48, dnPKA: N=3, n=146, CREdnPKA: N=3, n=86)

F) Maximal distance between nucleus and centrosome during CK of neurons electroporated with centrin-RFP and GFP or dnPKA-GFP in Kif3a$^{lox/lox}$ background. The black line represents the median. (One-way Kruskal-Wallis test (Chi square X^2= 8.11, $p < 0.001$, df = 3, followed by Nemenyi test (** $p < 0.01$), GFP: N=3, n=50, dnPKA: N=3, n=86)

G) Percentage of CK efficiency in neurons electroporated with centrin-RFP and GFP or dnPKA-GFP in Kif3a$^{lox/lox}$ background. (Pearson's Chi-squared test X^2= 6.06, p-value =0.027, GFP: N=3, n=50, dnPKA: N=3, n=86)

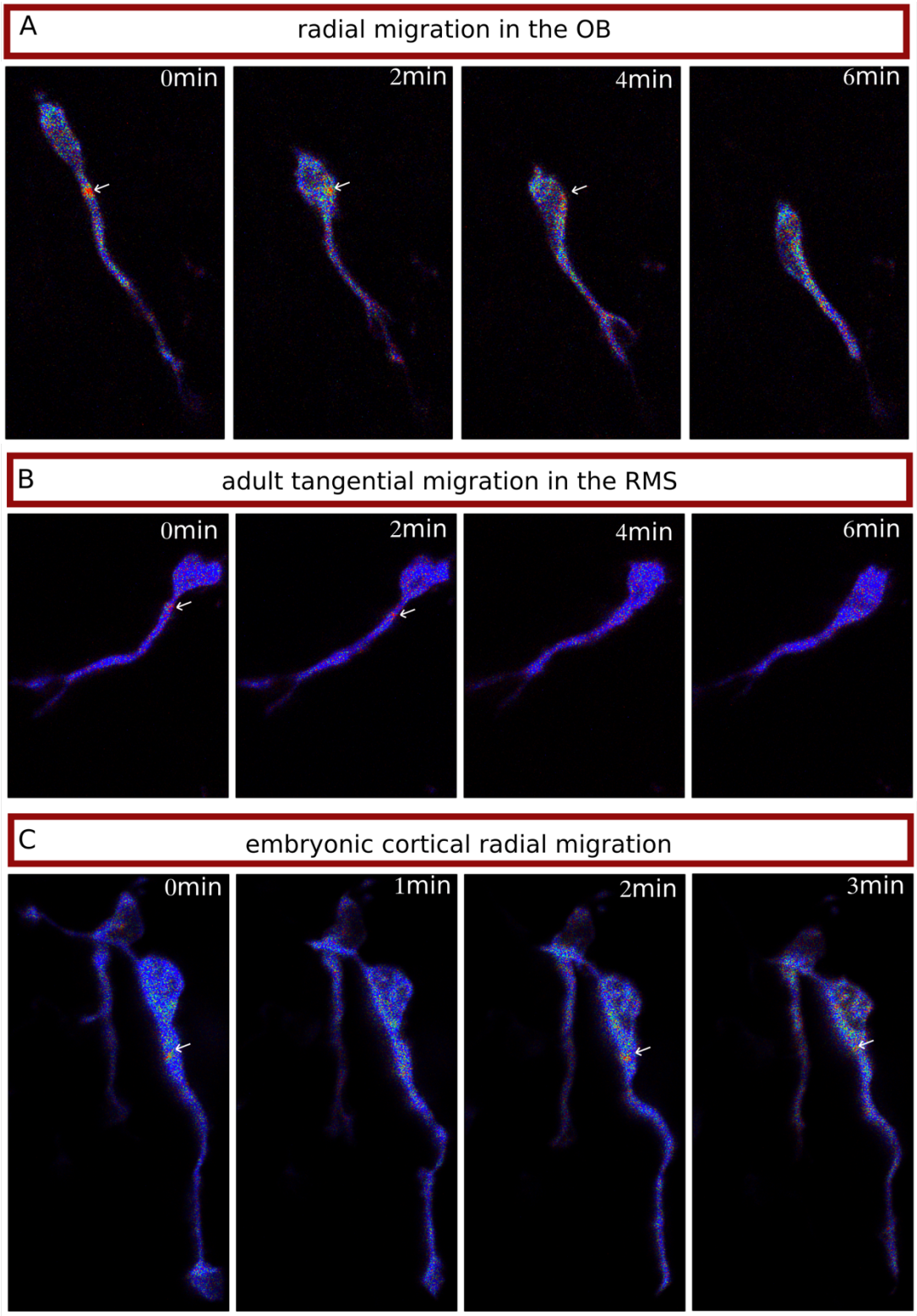

Figure 7: **The cAMP hotspot is present in different kind of migrating neurons**

A) Live biphotonic imaging of a radially migrating neuron in the olfactory bulb transfected by Epac-S^{H18}7. The cAMP hotspot is present during NK.

B) Live biphotonic imaging of a tangentially migrating neuron in the adult RMS transfected by Epac-S^{H18}7. The cAMP hotspot is present during NK.

C) Live biphotonic imaging of a radially migrating neuron in the embryonic cortex transfected by Epac-S^{H18}7. The cAMP hotspot is present during NK.

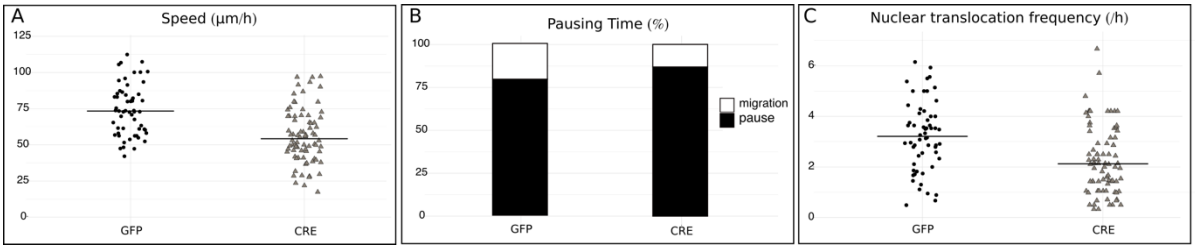

Figure S1: **Migration defects after primary cilium ablation in Rpgrip1l$^{lox/lox}$ mice**

A) Average speed of neurons electroporated with GFP or CRE-GFP in Rpgrip1l$^{lox/lox}$ background. The black line represents the median. (student test t(136) = 4.86, p<0.001,GFP: N=4, n=58, CRE: N=3, n=80)

B) Percentage of pausing time of neurons electroporated with GFP or CRE-GFP in Rpgrip1L background. (GFP: N=4, n=58, CRE: N=3, n=80) (Pearson's Chi-squared test X^2= 48.66, p-value < 0.001)

C) Nuclear translocation frequency of neurons electroporated with GFP or CRE-GFP Rpgrip1l background. The black line represents the median. (Mann-Whitney test U (136) = 3.01, p= 0.03, GFP: N=4, n=58, CRE: N=3, n=80)

Supplementary Material and Methods (figure 7)

In utero electroporation

Timed pregnant E15 C57Bl6 mice were anesthetized with isoflurane. During the experiment, mice were on a 37°C plate. The uterine horns were exposed, and the embryos were injected in the lateral ventricle with a glass micropipette. 1µL of plasmid (2µg/µL) was injected. The successfully injected animals were then subjected to 5pulses of 45V during 50ms separated by 950ms using the CUY21 SC Electroporator and 5mm tweezer electrode (CUY650-5 Nepagene). The uterine horns were then replaced in the belly and the belly was sewn up. The animals were placed in a cage on 37°C plates to restore their body temperature before returning in their own cage.

Adult electroporation

P21 C57Bl6 animals were anesthetized with a mixture of ketamine and xylazine. Stereotaxic injection (from the bregma M/L: 1, A/P:0, D/V:2,1) was performed with a glass micropipette and 2µL of the plasmids (10µg/µL) was injected in the right lateral ventricle. The animals were then removed from the stereotaxic setting and subject to 5 pulse of 200V during 50ms space out of 950ms using the electroporator NEPA21 with 10mm tweezer electrode (CUY650-10). The animals were then placed on a 37°C plates to restore their body temperature before returning in their cage.

Acute brain slices

For imaging of E18 embryos, the mother was killed by cervical dislocation and the embryos were removed from the horn and placed in an ice-cold cutting solution (same composition as above). The embryos were decapitated, and the brain was quickly removed from the skull. 300µm sagittal brain slices were cut in the same ice-cold solution. Then the same protocol as above was followed.

P30 mice were killed by cervical dislocation. The brain was quickly removed from the skull. 200µm sagittal brain slices were cut with a VT1200S microtome (Leica). Slices were prepared in an ice-cold solution of the following composition: 130mM potassium gluconate, 15mM KCl, 2mM EGTA, 20mM HEPES, 25mM glucose, 1mM CaCl2 and 6mM MgCl2, supplemented with 0.05mM D-APV (304 mOsm, pH 7.4 after equilibration) saturated with

5% CO_2 and 95% O_2 (Quiquempoix et al., 2018). Then the slices were places for 3 to 5 minutes in a ice-cold solution of the following composition: 225mM D-mannitol, 2.5mM KCl, 1.25mM NaH2PO4, 25mM NaHCO3, 25mM glucose, 1mM CaCl2 and 6mM MgCl2 (Quiquempoix et al., 2018) saturated with 5% CO_2 and 95% O_2 before being placed in the recording solution (described above) at 32°C and saturated with 5% CO_2 and 95% O_2 for at least 30 min.